A microstructure-based model for describing the material property of Al-Zn alloys during high pressure torsion

M. Borodachenkova[a], F. Barlat[a,b], W. Wen[a,*], A. Bastos[a], J.J. Grácio[a]

[a]Center for Mechanical Technology and Automation, Mechanical Engineering Department, University of Aveiro, 3810 Aveiro, Portugal; [b]Graduate Institute of Ferrous Technology (GIFT), Pohang University of Science and Technology (POSTECH), San 31 Hyoja-dong, Nam-gu, Pohang, Gyeongbuk 790-784, Republic of Korea;

*Corresponding author: wwen@ua.pt
Tel. +351 234 370 827, Fax. +351 234 370953

ABSTRACT

In this work, super saturated solid solution Al-30wt%Zn alloy was subjected to High Pressure Torsion (HPT). The material property and microstructure evolution was experimentally studied. Despite of strong grain refinement during HPT, the softening process is observed. Such a mechanical behavior is captured by a proposed model (MBWG) that takes into consideration the effects of solid solution hardening, Orowan looping and evolution of the dislocation density. Namely, the softening process occurred during HPT is attributed to decomposition of super saturated solid solution and evolution of the dislocation mean free path with plastic strain. Our simulation shows that the proposed model describes well the softening and saturation processes, and the decomposition of solid solution plays a significant role during HPT process.

Keywords: Al-Zn alloys, Grain refinement, High Pressure Torsion, Modeling, Precipitates, Solid solution hardening

Outline

1. INTRODUCTION

Several techniques of severe plastic deformation (SPD) such as equal channel extrusion, asymmetric rolling and high pressure torsion (HPT) have been developed to improve the mechanical properties of metals (Segal, 1995; Valiev et al., 2000; Valiev and Langdon, 2006; Khan and Meredith, 2010; Meredith and Khan, 2012; Seipp et al., 2012). Among these techniques, HPT is especially effective to introduce extremely large shear strain due to the occurrence of strong grain refinement (Valiev and Alexandrov, 1999; Zhilyaev et al., 2003; Zhilyaev and Langdon, 2008). The HPT process has been the subject of many investigations as a new method of processing for nanostructured materials due to its ability to develop homogeneous nanostructures with high-angle grain boundaries (Valiev et al., 2003; An et al., 2010). The effect of HPT on the mechanical behavior and the alterations of microstructural features have been investigated extensively on a wide range of pure and alloyed metals (Islamgaliev et al., 1997; Mishra et al., 1998; Zhilyaev et al., 2001; Zhilyaev et al., 2003; Sakai et al., 2005; Zhilyaev et al., 2005; Lugo et al., 2008; Edalati et al., 2008, 2009; Todaka et al., 2008; Ito and Horita, 2009; Edalati et al., 2011; Edalati and Horita, 2011; Ni et al., 2011; Srinivasarao et al., 2013). The previous investigations have shown that the application of HPT to aluminum-based alloys leads to both small grain size and high level of microhardness (Wang et al., 1996; Stolyarov et al., 1997; Islamgaliev et al., 2001; Gubicza et al., 2007, Loucif et al., 2010; Valiev et al., 2010; Zhang et al., 2010; Ghosh et al., 2012; Tugcu et al., 2012; Sabirov et al., 2013). In the work of Islamgaliev et al. (2001), the nanostructured Al-Zn-Cu-Mg-Zr alloy after HPT demonstrated a tensile strength (up to 800 MPa). Y. Harai et al. (2009) and C. Xu et al. (2007) have investigated the evolution of the mechanical behavior for pure aluminum during the HPT process. The results show that the hardness of pure Al initially

increases with increasing strain, and then, after reaching a maximum value, decreases to a constant level. Xu et al. (2007) attributed the unusual softening phenomenon at large strain to the easy cross-slip and the dynamic recovery due to the large stacking fault energy (SFE) of Al.

Despite a lot of studies have been carried out on HPT, most of them are only dedicated to the microstructure evolution and mechanical characterization (Zhilyaev and Langdon, 2008). However, in the past few years, many researchers have attempted to develop various dislocation models to describe the microstructural evolutions under large imposed strains (Langlois and Berveiller, 2003; Khan et al., 2006; Khan and Farrokh, 2006; Beyerlein and Tomé, 2007; Mayama et al., 2007; Farrokh and Khan, 2009; Groh et al., 2009; Starink et al., 2009; Austin and McDowell, 2011; Li and Soh, 2012; Ostapovets et al., 2012; Oppedal et al., 2012; Aoyagi et al., 2013; Bertin et al., 2013; Hansen et al., 2013; Kitayama et al., 2013; Lee et al., 2013; Wen et al., 2013). In the physically-based model developed by Starink et al. (2013) it was possible to predict the increment of hardness and grain refinement of pure metals during HPT process. This model takes into account the dislocation and the grain boundary strengthening by incorporating the volume-averaged thermally activated dislocation annihilation and the grain boundary formation.

The most common models of the grain refinement due to large strain, particularly under HPT, are usually based on the notion that the dislocation cell structure, which forms in the early stage of plastic deformation, gradually transforms to a fine grain structure. This type of models are based on the approach of Kocks and Mecking (2003), which describes the deformation behaviour of metals and alloys in terms of a single internal variable, namely, the total dislocation density. Estrin et al. (1998)

proposed a constitutive model that describes the hardening behaviour of cell-forming crystalline materials at large strains. This model considers the evolution of the dislocation densities in the cell walls and the cell interiors. Zhang et al. (2011) developed a microstructural model that is based on the evolution of geometrically necessary dislocations and statistically stored dislocations that incorporates grain refinement. A key element of this model is the assumption that, at the very high strains developed in HPT, the dislocation density reaches a saturation value.

In a previous work (Mazilkin et al., 2012), it was shown that HPT of Al-30wt%Zn alloy induces a strong grain refinement. Surprisingly, the corresponding mechanical behavior consists in a continuous strain softening. Strain softening is usually found during hot working as a result of dynamic recovery and dynamic recrystallization. However, at room temperature, occurrences of the softening were recently reported in metals subjected to SPD and were attributed to the occurrence of concomitant phenomena such as dynamic recovery, dynamic recrystallization, high-angle grain boundary development and supersaturated solid solution decomposition (Mazilkin et al., 2012). However, the existing models are not able to connect the flow stress with the observed microstructure evolution.

In a previous work, Borodachenkova et al. (2013) made an attempt to develop a new microstructure-based model to explain the softening during HPT. The model consisted in two main components: (i) In the first stage of plastic deformation, the mechanical behavior is dictated by the gradual increase of the dislocation mean free path resulting from precipitation, and diffusion of Zn atoms towards the grain boundary; (ii) In the second stage, further grain refinement to nanoscale size promotes a dramatic increase in strain rate due to the diffusion-driven grain-boundary sliding according to the

theory of Raj and Ashby (1971). However, with this model, the contribution of different strengthening mechanisms was not evaluated.

The purpose of this paper is to explain with a microstructure-based model the evolution of the critical resolved shear stress with the accumulated shear strain during the HPT process. This model takes into account the contribution of different strengthening mechanisms such as dislocation multiplication, Orowan and solid solution hardening. The model is based on the understanding of microstructural evolution and the interaction of dislocations with the microstructure essential features.

2. EXPERIMENTAL DETAILS

Al-30wt%Zn alloy was prepared by induction melting in vacuum from high purity elements (5N Al and 5N5 Zn). After melting, the alloy was poured in vacuum into the water-cooled copper crucible with an internal diameter of 10 mm. Samples of the alloy were cut by spark machining in the disks with a thickness of about 1mm and diameter of 10mm, and then polished mechanically to a thickness of 0.38 mm. The principle of HPT is described in several articles (Vorhauer and Pippan, 2004; Horita and Langdon, 2005; Zhilyaev et al., 2005). The HPT process was conducted under quasi-constrained conditions. Fig. 1 illustrates the schematic of quasi-constrained HPT, where the outer flow of the disk-shaped sample nearby its peripheries is limited. A disk-shaped sample placed in the depression between massive anvils and is subjected to torsional straining under a high hydrostatic pressure of the order of several GPa. The HPT process in this work was performed at room temperature and conducted under an applied pressure, P, of 6.0 GPa for 0.2, 0.5, 0.7 and 1 anvil revolutions at a constant angular velocity of 1 rpm. During the processing, the main volume of the material is deformed in conditions of quasi-hydrostatic compression

under an applied pressure. As a result, in spite of the large strain values, the deformed sample is not destroyed.

The HPT equipment allows the direct measurement of the applied torque. The shear stress is then calculated using the following relation:

$$\tau = \frac{1}{M_\tau}\frac{3Q}{2\pi R^3} \quad (1)$$

where Q is the measured torque. R is the radius of the sample. M_τ is the Taylor factor for torsion whose value has been taken 1.65.

The shear strain of the disk subjected to HPT, γ, was calculated as:

$$\gamma = 2\pi RN/h \quad (2)$$

where N is the number of rotations, R the distance from the center of the sample and h the thickness of the disk (Estrin et al., 2008).

The Von Mises strain could be calculated as follow:

$$e_{eq} = \frac{\gamma}{\sqrt{3}} = \frac{2\pi RN}{h\sqrt{3}} \quad (3)$$

However, in this work, the axial strain was not considered.

All samples for structural investigations were cut from the deformed disks at a distance of 2.5 mm from the sample center. Transmission electron microscopy (TEM) investigations were carried out using a JEM-4000FX microscope operating at 400 kV. The TEM samples were prepared by electrochemical polishing. The X-ray diffraction analysis (XRDA) was used to investigate the phase composition on a SIEMENSD-

500 diffractometer ($CuK\alpha_1$ radiation). The precision X-ray reflection angle in a range of $2\theta > 100^o$ is used to determine the lattice parameters of the alloys by the Nelson-Riley procedure (Nelson and Riley, 1945).

The dislocation density was measured using X-ray diffraction line profile analysis. The conventional Multiple Whole Profile (MWP) fitting procedure, which is described in detail the work of Ungár et al. (2001), is used to evaluate the diffraction peak profiles. The procedure may be used to estimate the density of dislocations (ρ).

Hardness measurements were performed also at 2.5 mm from the center, using a nanoindenter (MTS Nano Instruments, Inc., Oak Ridge, TN). The system has load and displacement resolutions of 50 nN and 0.01 nm, respectively.

3. EXPERIMENTAL RESULTS

3.1 Material property

The experimental shear stress-shear strain curve of the Al-30wt%Zn alloy measured during the HPT processes is illustrated in Fig. 2. After a short positive strain hardening regime (up to 1.3), strain softening was detected until 26 plastic shear strain, after which a steady state is observed. The experimental shear stress values have been compared with hardness measurements (Fig. 3) carried out at different strain levels and a good qualitative agreement was observed.

3.2 Microstructure evolution

The microstructural evolution of Al-30wt%Zn obtained by TEM is shown in Fig. 4. The microstructure presents the isolated ellipsoid black grains of (Zn) solid solution among the gray grains of (Al) solid solution. Fig. 4 shows that the alloy contains Al and Zn grains with average sizes of 15 and 1 μm, respectively (Fig. 4a). The Zn grains

are decorating the Al grain boundaries and present an ellipsoid shape. In the first stage of deformation (until the shear strain of 10.5), a strong precipitation of Zn occurs in the bulk and at the Al grain boundaries. In addition, the pinned dislocations self-organized structures give rise to highly misoriented grain boundaries (new grains) (Fig. 4b). With increasing strain, the Zn precipitates grow in size (from about 20 to 60 nm) and the Zn atoms diffuse and reform grain boundary precipitates (Fig 4c, 4d). At shear strain of 52 (Fig. 4e), the bulk of Al grains is almost free of precipitates and dislocations, which indicates that the intensive recovery has occurred.

TEM observations suggest that dislocations in the bulk of Al and grain boundaries serve as nucleation sites for Zn precipitates. Before the deformation, Zn concentration is high and the solid solution is highly super-saturated. With increasing deformation, the dislocations rearrange and self-organize to form new grain boundaries which become heavily enriched in Zn. The dislocations pinned at precipitates contribute Zn redistribution by pipe diffusion. In addition, the intense pinning produces an effective division of the grains leading to sub-grain boundaries, which contribute to an even higher rate of solute diffusion towards the growing precipitates. In this way, Zn concentration in Al decreases due to dislocation motion into the sub-grain boundaries, which controls the softening process. It is well known, for solute, that the grain boundary and pipe diffusions are much faster than the bulk diffusion. The schematic view of the grain refinement for Al-Zn alloys during HPT processes is presented in Fig. 5.

3.3 Grain size and lattice parameter measurements

The evolution of the grain size with the shear strain for Al and Zn grains is illustrated in Fig. 6. After shear strain up to 10.5, the grain sizes of Al and Zn decrease,

respectively to 1.2 μm and 0.43 μm. Further deformation resulted in grain refinement down to 0.55 μm after shear strain of 36.5.

It is well-known that in a super saturated solid solution Al-Zn alloy, the lattice parameter of aluminum is strongly influenced by Zn atoms. The XRD analysis of Al-Zn alloys before and after HPT shows that it contains two phases, namely (Al) solid solution and (Zn) solid solution grains. According to the equilibrium phase diagram, the Al-Zn alloys contain two phases at room temperature: (Al) solid solution with Zn content less than 0.5 wt% and (Zn) solid solution with Al content less than 0.1 wt%. Due to the intensive occurrence of precipitation during HPT, the lattice parameter of Al should also increase during the process. The values of the lattice parameter for Al-based solid solution at different shear strains are listed in Table 1. It can be seen that the lattice parameter increases until a shear strain of 26 (value close to that of pure Al). In our case, the supersaturated solid solution with an initial concentration of 17 wt% decomposes completely after shear strain of 26.

4. MICROSTRUCTURE-BASED MODEL (MBWG)

According to the previous observation, it is assumed that the total strength of Al-Zn alloy is expressed as

$$\tau - \tau_{ss} = \tau_{dis} + \tau_{Orowan} \quad (4)$$

where τ_{ss} , τ_{dis} and τ_{Orowan} are the strengthening related with solid solution, dislocation density and Orowan mechanism, respectively.

4.1 Precipitation hardening

The importance of τ_{Orowan} was well illustrated by the microstructural analysis revealing that during the first steps of plastic deformation (until shear strain of 10.5), Al grains contain a population of small Zn-rich precipitates, which were assumed to impede the motion of dislocations. In the present approach, τ_{Orowan} is supposed to depend on both the Zn precipitate inter-spacing (ω) and their size (d) according to the following expression (Kocks, 1966; Gubicza et al., 2007):

$$\tau_{Orowan} = k_{or} \frac{0.85\mu b ln\left(\frac{d}{b}\right)}{2\pi\left(\omega - d\right)} \tag{5}$$

According to the experimental measurement, the Zn precipitates grow in size (from about 20 to 60 nm); the distance between participates also evolves between 300 nm and 600 nm. k_{or} is introduced in Eq. (5) to describe approximately τ_{Orowan} evolution for the initial step of the deformation and to eliminate its contribution after the shear strain of 10.5 because the strong Zn precipitations only occurs in the bulk of Al grains at the beginning of the plastic deformation. In this work, k_{or} is imposed to be increased linearly from 0 to 1 until the shear strain of 1.3, and then decreased linearly to 0 until the shear strain of 10.5.

4.2 Dislocation hardening

The contribution of dislocation hardening is assumed to depend on the average dislocation density (the same in every grain) through the usual Taylor law:

$$\tau_{dis} = \alpha\mu b\sqrt{\rho} \tag{6}$$

where α is a dislocation-dislocation interaction coefficient, μ the elastic shear modulus, b the Burgers vector and ρ the dislocation density.

In the approach proposed by Kocks and Mecking (2003), the annihilation process is thermally activated and governed by the glide of dislocations at low and medium temperature regimes. Thus, the evolution of the dislocation density with shear strain is given by:

$$\frac{d\rho}{d\gamma} = \frac{1}{bL} - f\rho - k_e\rho \tag{7}$$

where $k_e = (d_e / d)^2$. d_e is a reference grain size corresponding to the critical grain size at which enhanced dynamic recovery occurs, and d is the grain size. The critical grain size for Al alloy is around 1 μm (Hariprasad et al., 1996). L is the dislocation mean free path and f a recovery term.

In the present formulation, L is considered as an independent state variable that evolves with shear deformation as shown in Eq. (8).

$$\frac{dL}{d\gamma} = d_{\mathrm{sat}} e^{-m\gamma} - d_{\mathrm{r}} e^{-n\gamma} \tag{8}$$

where d_{sat} is the saturation grain size. m and n are fitting constants. d_r identifies the representative distance between Zn precipitates during the HPT processes which is approximately calculated by $d_r = \frac{L_{max} + \omega_i}{2}$ in this work. ω_i and L_{max} are respectively the initial and maximum Zn precipitate interspacing during the HPT processes.

Unlike in the Kocks-Mecking original approach, here the mean free path is first assumed to be determined by the precipitate interspacing and, after some amount of

plastic deformation, by the refined grain size. Indeed, as discussed in the next section, L should be significantly lower than the mean free path of the original Kocks-Mecking model, which is totally due to dislocation interspacing, thus, proportional to $1/\sqrt{\rho}$. The two terms on the right side of Eq. (8) characterize two of the main physical processes involved in the plastic deformation process: Orowan looping controlled by the distance between precipitates and the saturation grain size.

Integration of Eq. (8) leads to the following expression for L:

$$L = \int \frac{dL}{d\gamma} = \int d_{\mathrm{sat}} e^{-m\gamma} - \int d_{\mathrm{r}} e^{-n\gamma} = -\frac{d_{\mathrm{sat}}}{m} e^{-m\gamma} + \frac{d_{\mathrm{r}}}{n} e^{-\mathrm{n}\gamma} + c_i \tag{9}$$

where c_i is an integration constant. According to the microstructural observations, it is clear that when $\gamma \to \infty$, $L \to d_{sat}$, and therefore $c_i = d_{sat}$. Under this circumstance we obtain:

$$L = -\frac{d_{\mathrm{sat}}}{m} e^{-m\gamma} + \frac{d_{\mathrm{r}}}{n} e^{-\mathrm{n}\gamma} + d_{sat} \tag{10}$$

4.3 Solid solution hardening

It is well-known that solid solution strengthening is related with the interactions of gliding dislocations with solute atoms and is highly sensitivity to the temperature. In order to describe such an effect, Kocks and Mecking (1981) proposed a model based on a thermally activated stress component. In the present work, a modified version of this approach is introduced which is dependent on the Zn atom concentration in Al and a thermal component as proposed in the original version.

$$\tau_{\mathrm{ss}} = k_1 \left[\tau_0 + a_0(c) \left[1 - \left(\frac{\mathrm{kT}}{\Delta \mathrm{G}} ln \frac{\dot{\gamma}_0}{\dot{\gamma}} \right)^{2/3} \right] \right] \tag{11}$$

where τ_0 is the friction stress, k the Boltzmann constant, T the temperature, ΔG the activation energy for deformation. $\dot{\gamma}_0$ is the characteristic strain rate which is related to the vibrational frequency of dislocations arrested at an obstacle or, alternatively, the attempt frequency for overcoming an obstacle (Kocks et al., 1975). k_1 is introduced in Eq. (11) to approximately describe the evolution of τ_{ss} for the initial step of deformation. This parameter is imposed to be linear increasing from 0 to 1 at the beginning of the deformation, and remain to be 1 during the softening process. a_0 is the value of thermal stress at 0 K dependent on the Zn concentration in Al grains (c). An expression of a_0 is proposed based on the analysis of Zaiser (2002) and Olmsted et al., (2006):

$$a_0 = \tau_p + \frac{3\Lambda}{2b^3}\left(\frac{\sqrt{2}\hat{U}^4}{A\omega_0}\right)^{1/3}\sqrt{c} \tag{12}$$

where τ_p is the Peierls stress, $\hat{U}$ the characteristic interaction energy between a single solute and a straight dislocation, Λ an adjustable scaling factor, ω_0 the characteristic range for the interaction, and A the line tension energy per unit length of dislocation which can be expressed as (Soare and Curtin, 2008):

$$A = \frac{3\mu b^2}{4\pi(1-\nu)} \tag{13}$$

here ν is the Poisson ratio.

Based on the lattice parameter measurements and the relationship between this parameter and Zn concentration in Al grain investigated in the work of Ellwood (1952), the intensity of solid solution decomposition was evaluated by determining

the evolution of Zn concentration in Al during HPT. The concentration evolution was described as:

$$c=c_1 exp\left(-c_2\gamma\right)-c_3 exp\left(-c_4\gamma\right)+c_{sat} \quad (14)$$

where c_1 , c_2 , c_3 and c_4 are fitting parameters, and c_{sat} is the equilibrium Zn concentration in Al grains.

5. Discussion

In order to calculate the dislocation mean free path L, the coefficients m and n in Eq. (8) need to be determined. For that, several boundary conditions should be introduced. First, based on TEM observations (Fig. 4), it was possible to verify that the value of L obtained for $\gamma=\gamma_1\approx 10.5$ is about 600 nm (L_{max}). Such a condition can be expressed by:

$$-\frac{d_{sat}}{m}e^{-m\gamma}+\frac{d_r}{n}e^{-n\gamma}+d_{sat}=L_{max} \quad (15)$$

Second, when $\gamma=0$, Eq. (10) becomes:

$$-\frac{d_{\mathrm{sat}}}{m}+\frac{d_{\mathrm{r}}}{n}+d_{sat}=\omega_{\mathrm{i}} \quad (16)$$

Eqs. (15, 16) enable the calculation of the parameters m and n in Eq. (8) which are listed in Table 2. Then, the evolution of L with plastic strain is shown in Fig. 7. By considering the evolution of L and integrating Eq. (7), the dislocation density is obtained as a function of the plastic strain (see Fig. 8). It can be seen that the dislocation density increases at the beginning of the plastic deformation, then decreases dramatically until a shear strain around 10.5 and finally keeps a steady

value. Due to the intense annihilation process verified at the beginning of HPT, an unusual high recovery parameter f of 6330 has to be considered to get a good approximation between model and experiment.

As mentioned in section 4, the Kocks-Mecking model suppose that L is determined only by the dislocation interspacing, whereas the MBWG model assumes that the evolution of L is due to the precipitate interspacing, and the refined grain size after certain plastic deformation. In this case, the L calculated by the MBWG model should be much lower than the one of Kocks-Mecking model. To validate this point, we propose a comparison of L determined by both models. According to the Kocks and Mecking approach, the dislocation mean free path is inversely proportional to the square-root of the dislocation density:

$$\frac{1}{L_{K-M}} = \frac{\sqrt{\rho}}{K} + \frac{1}{D} \tag{17}$$

with K the number of forest dislocations a moving segment is able to cross before being trapped by the obstacles. D is the initial grain size of Al. In the present work, the exact value of K for Al-30wt%Zn alloy cannot be obtained. Therefore, we select several values of K between the minimum value ($K = 1$) and the value of $K = 30$ which is suggested for AA 6022-T4 by literature (Rauch et al., 2007). The calculated mean free paths with Eqs. (8) and (17) are shown in Fig. 9. The results with high K value have no physics sense because they exceed the measured initial grain size of Al (see Fig. 6). However, we can notice that, for all the K values, the mean free path calculated with the Kocks-Mecking approach is much larger than that obtained with the MBWG model. This suggests that during HPT of Al-Zn alloys, the dislocation mean free path is mainly controlled by the density of precipitates, and then, by the

refined grain size. In contrast, the dislocation density has a minor effect on the mean free path.

The evolution of τ_{dis} with shear strain shown in Fig. 10 is calculated according to Eq. (6). It can be seen that such a low dislocation density produces a maximum τ_{dis} around 3 MPa. This means that the dislocation density strengthening mechanism does not play a significant role during HPT process of Al-Zn alloy.

In the calculation of Zn concentration in Al, the parameters in Eq. (14), which is listed in Table 2, is determined from a fitting process to experimental results. The simulated and experimental Zn concentrations are shown in Fig. 11. Based on this, the evolution of the solid solution stress can be calculated by Eqs. (11-14). In those equations, the Peierls stress is suggested to be $\tau_p \approx 3\,\mathrm{MPa}$ (Soare and Curtin, 2006). In the analysis of Olmsted et al. (2006) for Al-Mg alloys, the value of $\hat{U}$ and Λ have been determined to be around 0.1 eV and 2, respectively, and ω_0 is belongs to the range between 10~20 $\mathring{\mathrm{A}}$. In the present work, the value of $\hat{U}$ and ω_0 are adapted for Al-Zn alloys by a fitting process, and all the parameters in Eqs. (11-14) are listed in Table 2. The calculated evolution of τ_{ss} is presented in Fig. 12. The comparison of the contribution of the hardening mechanisms are presented in Fig. 13. We should note that the values of τ_{ss} is much higher than τ_{dis} and τ_{Orowan}.

On the basis of the previous analysis, it is possible to calculate the stress-strain curves using Eq. (4). The curve predicted by the MBWG model is presented and compared with experimental result in Fig. 14. It can be seen that the MBWG model can describes well both the softening and saturation processes during HPT. Moreover, the

calculation indicates that the softening process is mostly associated with a strong decrease of τ_{ss} due to the depletion of Zn atom solutes in the Al grains.

6. CONCLUSIONS

In the present work, the material properties of Al-30wt%Zn alloy deformed under High Pressure Torsion (HPT) have been studied. It has been shown that HPT leads to a strong softening process at the beginning of plastic deformation. The material property has been compared with the microstructural evolution. It has been shown that the fundamental phenomena of the process are solid solution decomposition, Orowan looping and dislocation density, respectively. The material property is dictated at the beginning of plastic deformation by the decomposition of supersaturated solid solution and after saturation strain by saturation grain size.

The softening process has been well captured with a new model called MBWG that is based on strain induced diffusivity of Zn in Al grains and the evolution of the dislocation mean free path with plastic strain. The model considers the material property to be determined by the gradual increase in the mean free path of dislocations resulting from precipitation and diffusion of Zn atoms towards the grain boundaries. Further grain refinement at nanoscale promotes the saturation of dislocation mean free path and a transition to a grain boundary shearing dominant mechanism.

The calculated results by MBWG model present a good agreement with experiment. This model shows the capability to describe both the softening and saturation processes. The calculated shear stress evolution is mostly contributed by the solid solution shear stress. This suggests that the decomposition of super saturated solid solution plays the dominated role in the material property of Al-30wt%Zn alloy. The

MBWG model allows evaluate the contribution of the different strengthening mechanisms during the deformation and it can be adapted to other softening processes during plastic deformation.

ACKNOWLEDGMENTS

MB, FB, WW, AB and JG acknowledge the financial support of Portuguese Foundation of Science and Technology projects PTDC/EME-TME/105688/2008 and PEST-C/EME/UI0481/2011. The authors thank Professor R.C. Picu (Rensselaer Polytechnic Insitute) for the fruitful discussion and suggestions.

REFERENCES

An, X.H., Wu, S.D., Zhang, Z.F., Figueiredo, R.B., Gao, N., Langdon, T.G., 2010. Evolution of microstructural homogeneity in copper processed by high-pressure torsion. Scripta Mater. 63, 560-563.

Austin, R. A., McDowell, D. L., 2011. A dislocation-based constitutive model for viscoplastic deformation of fcc metals at very high strain rates. Int. J. Plasticity 27, 1-24.

Aoyagi, Y., Kobayashi, R., Kaji, Y., Shizawa, K., 2013. Modeling and simulation on ultrafine-graining based on multiscale crystal plasticity considering dislocation patterning, Int. J. Plasticity 47, 13-28.

Beyerlein, I.J., Tomé, C.N., 2007. Modeling transients in the mechanical response of copper due to strain path changes. Int. J. Plasticity 23, 640-664.

Borodachenkova, M., Gracio, J., Barlat, F., Picu, C.R., 2013. Transient negative strain hardening during severe plastic deformation of Al-30wt%Zn alloys. Key Engineering Materials, 554-557, 3-11.

Bertin, N., Capolungo, L., Beyerlein, I.J., 2013. Hybrid dislocation dynamics based strain hardening constitutive model. Int. J. Plasticity 49, 119-144.

Edalati, K., Yamamoto, A., Horita, Z., Ishihara, T., 2011. High-pressure torsion of pure magnesium: Evolution of mechanical properties, microstructures and hydrogen storage capacity with equivalent strain. Scripta Mater. 64, 880-883.

Edalati, K., Horita, Z., 2011. Significance of homologous temperature in softening behavior and grain size of pure metals processed by high-pressure torsion. Mater. Sci. Eng. A 528, 7514-7523.

Edalati, K., Fujioka, T., Horita, Z., 2008. Microstructure and mechanical properties of pure Cu processed by high-pressure torsion. Mater. Sci. Eng. A497, 168-173.

Edalati, K., Horita, Z., Yagi, S., Matsubara, E., 2009. Allotropic phase transformation of pure zirconium by high-pressure torsion. Mater. Sci. Eng. A 523, 277-281.

Ellwood, E.C., 1952. J. Inst. Met.74, 721.

Estrin, Y., Tóth, L.S., Molinari, A., Bréchet, Y., 1998. A dislocation-based model for all hardening stages in large strain deformation. Acta Mater. 46, 5509-5522.

Estrin, Y., Molotnikov, A., Davies. C.H.J., Lapovok, R., 2008. Strain gradient plasticity modelling of high-pressure torsion. J. Mech. Phys. Solids 56, 1186-1202.

Farrokh, B., Khan, A.S., 2009. Grain size, strain rate, and temperature dependence of flow stress in ultra-fine grained and nanocrystalline Cu and Al: Synthesis, experiment, and constitutive modeling. Int. J. Plasticity 25, 715-732.

Ghosh, K.S., Gao, N., Starink, M.J., 2012. Characterisation of high pressure torsion processed 7150 Al-Zn-Mg-Cu alloy. Mater. Sci. Eng A552, 164-171.

Groh, S., Marin, E.B., Horstemeyer, M.F., Zbib, H.M., 2009. Multiscale modeling of the plasticity in an aluminum single crystal. Int. J. Plasticity 25, 1456-1473.

Gubicza, J., Schiller, I., Chinh, N.Q., Illy, J., Horita, Z., Langdon, T.G., 2007. The effect of severe plastic deformation on precipitation in supersaturated Al-Zn-Mg alloys. Mater. Sci. Eng. A 460-461,77-85.

Hansen, B.L., Beyerlein, I.J., Bronkhorst, C.A., Cerreta, E.K., Dennis-Koller, D., 2013. A dislocation-based multi-rate single crystal plasticity model. Int. J. Plasticity 44, 129-146.

Harai, Y., Edalati, K., Horita, Z., Langdon, T. G., 2009. Using ring samples to evaluate the processing characteristics in high-pressure torsion. Acta Mater. 57, 1147-1153.

Hariprasad, S., Sastry, S.M.L., Jerina, K.L., 1996. Deformation behavior of a rapidly solidified fine grained Al-8.5% Fe-1.2% V-1.7% Si alloy. Acta Mater. 44, 383-389.

Horita, Z., Langdon, T.G., 2005. Microstructures and microhardness of an aluminium alloy and pure copper after processing by high-pressure torsion. Mater. Sci. Eng. A 410-411, 422-425.

Islamgaliev, R.K., Chmelik, F., Kuzel, R.,1997. Thermal structure changes in copper and nickel processed by severe plastic deformation. Mater. Sci. Eng. A 234-236, 335-338.

Islamgaliev, R.K., Yunusova, N.F., Sabirov, I.N., Sergueeva, A.V., Valiev, R.Z., 2001. Deformation behavior of nanostructured aluminum alloy processed by severe plastic deformation. Mater. Sci. Eng. A 319-321, 877-881.

Ito, Y., Horita, Z., 2009. Microstructural evolution in pure aluminum processed by high-pressure torsion. Mater. Sci. Eng. A 503, 32-36.

Khan, A.S., Farrokh, B., 2006. Thermo-mechanical response of nylon under uniaxial and multi-axial loadings: Part I, Experimental results over wide ranges of temperature and strain rates. Int. J. Plasticity 22, 1506-1529.

Khan, A.S., Meredith, C.S., 2010. Thermo-mechanical response of Al 6061 with and without equal channel angular pressing (ECAP). Int. J. Plasticity 26 189-203.

Khan, A.S., Suh, Y.S., Chen, X., Takacs, L., Zhang, H.Y., 2006. Nanocrystalline aluminum and iron: Mechanical behavior at quasi-static and high strain rates, and constitutive modeling. Int. J. Plasticity 22, 195-209.

Kitayama, K., Tomé, C.N., Rauch, E.F., Gracio, J.J., Barlat, F., 2013. A crystallographic dislocation model for describing hardening of polycrystals during strain path changes. Application to low carbon steels. Int. J. Plasticity 46, 54-69.

Kocks, U.F., 1966. A statistical theory of flow stress and work-hardening. Philos. Mag. 13, 541-566.

Kocks, U. F., Argon, A.S., Ashby, M. F., 1975. Thermodynamics and kinetics of slip. Prog. Mater. Sci., 19, 1-271.

Kocks, U.F., Mecking, H., 2003. Physics and phenomenology of strain hardening: the FCC case. Prog. Mater. Sci. 48, 171-273.

Langlois, L., Berveiller, M., 2003. Overall softening and anisotropy related with the formation and evolution of dislocation cell structures. Int. J. Plasticity 19, 599-624.

Lee, M.G., Lee, J.W., Gracio, J.J., Vincze, G., Rauch, E.F., Barlat, F., 2013. A dislocation-based hardening model incorporated into an anisotropic hardening approach. Comp. Mater. Sci. 79, 570-583.

Li, J., Soh, A.K., 2012. Modeling of the plastic deformation of nanostructured materials with grain size gradient. Int. J. Plasticity 39, 88-102.

Loucif, A., Figueiredo, R. B., Baudin, T., Brisset F., Langdon T.G., 2010. Microstructural evolution in an Al-6061 alloy processed by high-pressure torsion. Mater. Sci. Eng. A 527, 4864-4869.

Lugo, N., Llorca, N., Cabrera, J.M., Horita, Z., 2008. Microstructures and mechanical properties of pure copper deformed severely by equal-channel angular pressing and high pressure torsion. Mater. Sci. Eng. A 477, 366-371.

Mazilkin, A.A., Straumal, B.B., Borodachenkova, M.V., Valiev, R.Z., Kogtenkova, O.A., Baretzky, B., 2012. Gradual softening of Al-Zn alloys during high pressure torsion. Materials Letters. 84, 63-65.

Mayama, T., Sasaki, K., Ishikawa, H., 2007. A constitutive model of cyclic viscoplasticity considering changes in subsequent viscoplastic deformation due to the evolution of dislocation structures. Int. J. Plasticity 23, 915-930.

Mecking, H., Kocks, U.F., 1981. Kinetics of flow and strain-hardening. Acta Metall., 29, 1865-1875.

Meredith, C.S., Khan, A.S., 2012. Texture evolution and anisotropy in the thermo-mechanical response of UFG Ti processed via equal channel angular pressing. Int. J. Plasticity 30-31, 202-217.

Mishra, R.S., Valiev, R.Z., McFadden, S.X., Mukherjee, A.K., 1998. Tensile superplasticity in a nanocrystalline nickel aluminide. Mater. Sci. Eng. A 252, 174-178.

Nelson, J.B., Riley, D.P., 1945. Proc. Phys. Soc. London 57, 160.

Ni, S., Wang, Y.B., Liao, X.Z., Alhajeri, S.N., Li, H.Q., Zhao, Y.H., Lavernia, E.J., Ringer, S.P., Langdon, T.G., Zhu, Y.T., 2011. Strain hardening and softening in a nanocrystalline Ni–Fe alloy induced by severe plastic deformation. Mater. Sci. Eng. A 528, 3398-3403.

Olmsted, D.L., Hector, L.G., Curtin, W.A., 2006. Molecular dynamics study of solute strengthening in Al/Mg alloys. J. Mech. Phys. Solids 54, 1763-1788

Oppedal, A.L., El Kadiri, H., Tomé, C.N., Kaschner, G.C., Vogel, S. C., Baird, J.C., Horstemeyer, M.F., 2012. Effect of dislocation transmutation on modeling hardening mechanisms by twinning in magnesium. Int. J. Plasticity 30-31, 41-61.

Ostapovets, A., Šedá, P., Jäger, A., Lejček, P., 2012. New misorientation scheme for a visco-plastic self-consistent model: Equal channel angular pressing of magnesium single crystals. Int. J. Plasticity 29, 1-12.

Raj, R., Ashby, M. F., 1971. On grain boundary sliding and diffusional creep. J. Metall. Trans. 2A, 1113-1117.

Rauch, E.F. Gracio, J.J., Barlat, F., 2007. Work-hardening model for polycrystalline metals under strain reversal at large strains. Acta Mater. 55, 2939-2948.

Sabirov, I., Murashkin, M.Yu., Valiev, R.Z., 2013.Nanostructured aluminium alloys produced by severe plastic deformation: New horizons in development. Mater. Sci. Eng. A 560, 1-24.

Sakai, G., Horita, Z., Langdon, T.G., 2005. Grain refinement and superplasticity in an aluminum alloy processed by high-pressure torsion. Mater. Sci. Eng. A 393, 344-351.

Segal V.M., 1995. Materials processing by simple shear. Mater. Sci. Eng. A 197, 157-164.

Seipp, S., Wagner, M.F.-X., Hockauf, K., Schneider, I., Meyer, L.W., Hockauf, M., 2012. Microstructure, crystallographic texture and mechanical properties of the magnesium alloy AZ31B after different routes of thermo-mechanical processing. Int. J. Plasticity 35, 155-166.

Soare, M.A., Curtin, W.A., 2008. Solute strengthening of both mobile and forest dislocations: The origin of dynamic strain aging in fcc metals, Acta Mater. 56, 4046-4061.

Srinivasarao, B., Zhilyaev, A.P., Langdon, T.G., Pérez-Prado, M.T., 2013. On the relation between the microstructure and the mechanical behavior of pure Zn processed by high pressure torsion. Mater. Sci. Eng. A 562, 196-202.

Starink M. J., Cheng X., Yang S., 2013. Hardening of pure metals by high pressure torsion: A physically based model employing volume-averaged defect evolutions. Acta Mater. 61, 183-192.

Starink, M. J., Qiao, X. G., Zhang, J., Gao, N., 2009. Predicting grain refinement by cold severe plastic deformation in alloys using volume averaged dislocation generation Acta Mater. 57 5796-5811.

Stolyarov, V.V., Latysh, V.V., Shundalov, V.A., Salimonenko, D.A., Islamgaliev, R.K., Valiev, R.Z., 1997. Influence of severe plastic deformation on aging effect of Al-Zn-Mg-Cu-Zr alloy. Mater. Sci. Eng. A 234-236, 339-342.

Todaka, Y., Sasaki, J., Moto, T., Umemoto, M., 2008. Bulk submicrocrystalline ω-Ti produced by high-pressure torsion straining. Scripta Mater. 59, 615-618.

Tugcu, K., Sha, G., Liao, X.Z., Trimby, P., Xia, J.H., Murashkin, M.Y., Xie, Y., Valiev, R.Z., Ringer, S.P., 2012. Enhanced grain refinement of an Al-Mg-Si alloy by high pressure torsion processing at 100 ^{o}C. Mater. Sci. Eng. A 552, 415-418.

Ungár, T., Gubicza, J., Ribárik, G. Borbély, A., 2001. Crystallite size distribution and dislocation structure determined by diffraction profile analysis: principles and practical application to cubic and hexagonal crystals. J. Appl. Cryst. 34, 298-310.

Valiev, R.Z., Enikeev, N.A., Murashkin, M.Yu., Kazykhanov, V.U., Sauvage, X., 2010. On the origin of the extremely high strength of ultrafine-grained Al alloys produced by severe plastic deformation. Scripta Mater. 63, 949-952.

Valiev R. Z., Langdon T.G., 2006. Principles of equal-channel angular pressing as a processing tool for grain refinement. Prog. Mater. Sci. 51, 881-981.

Valiev, R.Z., Islamgaliev, R.K., Alexandrov, I.V., 2000. Bulk nanostructured materials from severe plastic deformation. Prog. Mater. Sci. 45, 103-189.

Valiev, R.Z., Alexandrov, I.V., 1999. Nanostructured materials from severe plastic deformation. Nanostruct. Mater. 12, 35-40.

Vorhauer, A., Pippan, R., 2004. On the homogeneity of deformation by high pressure torsion. Scripta Mater. 51, 921-925.

Wang, J., Iwahashi, Y., Horita, Z., Furukawa, M., Nemoto, M., Valiev, R.Z., Langdon, T.G., 1996. An investigation of microstructural stability in an Al-Mg alloy with submicrometer grain size. Acta Mater. 44, 2973-2982.

Wen, W., M'Guil, S., Ahzi, S., Gracio, J.J., 2013. Coupled effects of the lattice rotation definition, twinning and interaction strength on the FCC rolling texture evolution using the viscoplastic ϕ-model. Int. J. Plasticity 46, 23-36.

Xu, C., Horita, Z., Langdon, T.G., 2007. The evolution of homogeneity in processing by high-pressure torsion. Acta Mater. 55, 203-212.

Zaiser, M., 2002. Dislocation motion in a random solid solution, Philos. Mag. A 82, 2869-2883.

Zhang, J., Gao, N., Starink, M. J., 2011. Microstructure development and hardening during high pressure torsion of commercially pure aluminium: Strain reversal experiments and a dislocation based model. Mater. Sci. Eng. A 528, 2581-2591.

Zhang, J., Gao, N., Starink, M.J., 2010. Al-Mg-Cu based alloys and pure Al processed by high pressure torsion: The influence of alloying additions on strengthening. Mater. Sci. Eng. A 527, 3472-3479.

Zehetbauer, M.J., Kohout, J., Schafler, E., Sachslehner, F., Dubravina, A., 2004. Plastic deformation of nickel under high hydrostatic pressure. J. Alloys Comp. 378, 329-334

Zhilyaev. A.P., Langdon, T.G., 2008. Using high-pressure torsion for metal processing: Fundamentals and applications. Prog. Mater. Sci. 53, 893-979.

Zhilyaev, A.P., Nurislamova, G.V., Kim, B.-K., Baró, M.D., Szpunar, J.A., Langdon, T.G., 2003. Experimental parameters influencing grain refinement and microstructural evolution during high-pressure torsion. Acta Mater. 51, 753-765.

Zhilyaev, A.P., Lee, S., Nurislamova, G.V., Valiev, R.Z., Langdon, T.G., 2001. Microhardness and microstructural evolution in pure nickel during high-pressure torsion. Scripta Mater. 44, 2753-2758.

Zhilyaev, A.P., Oh-ishi, K., Langdon, T.G., McNelley, T.R., 2005. Microstructural evolution in commercial purity aluminum during high-pressure torsion. Mater. Sci. Eng. A 410-411, 277-280.

FIGURE CAPTIONS

Fig. 1. Schematic illustration of quasi-constrained HPT setup

Fig. 2. Experimental shear stress-shear strain curve

Fig. 3. The hardness measurements at different strain level

Fig. 4. The microstructural evolution of Al-30wt%Zn during HPT, for the initial state (a) and at different strain level: (b)- $\gamma = 10.5$, (c)- $\gamma = 26$, (d)- $\gamma = 36.5$ and (e)- $\gamma = 52$

Fig. 5. Schematic view of grain refinement of Al-Zn alloys during HPT process.

Fig. 6. The evolution of the grain size with the shear strain

Fig. 7. The calculated evolution of the dislocation mean free path with shear strain

Fig. 8. The experimental and calculated evolutions of the dislocation density with shear strain

Fig. 9. The comparison of the evolution of dislocation mean free path with shear strain calculated by the approach of Kocks and Mecking (Eq. 17) and MBWG model (Eq. 8)

Fig. 10. The calculated evolution of the τ_{dis} shear stress with shear strain

Fig. 11.The evolution of Zn concentration in Al grains with shear strain

Fig. 12. The calculated evolution of τ_{ss} shear stress with shear strain

Fig. 13. The comparison of the contribution of different hardening mechanisms

Fig. 14. Comparison between the predicted and experimental shear strain-shear stress curves.

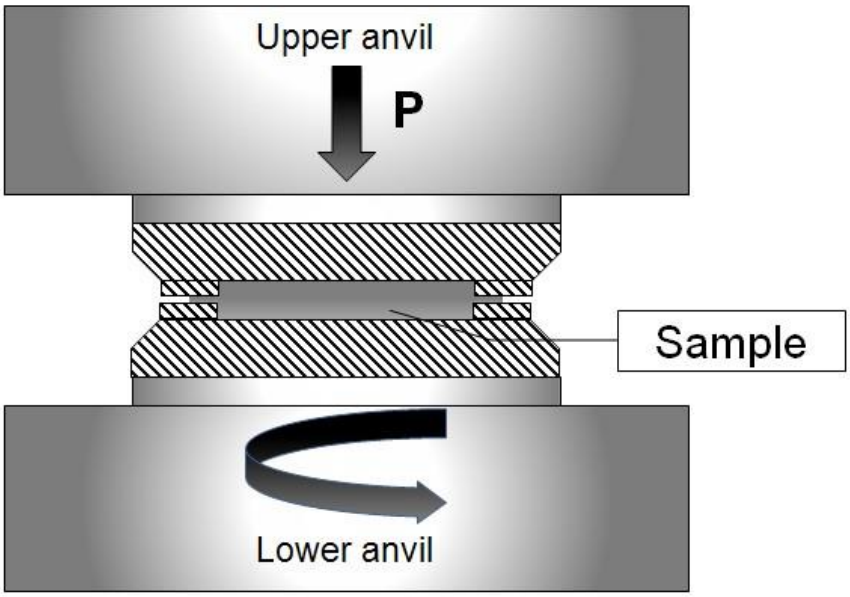

Fig. 1. Schematic illustration of quasi-constrained HPT setup

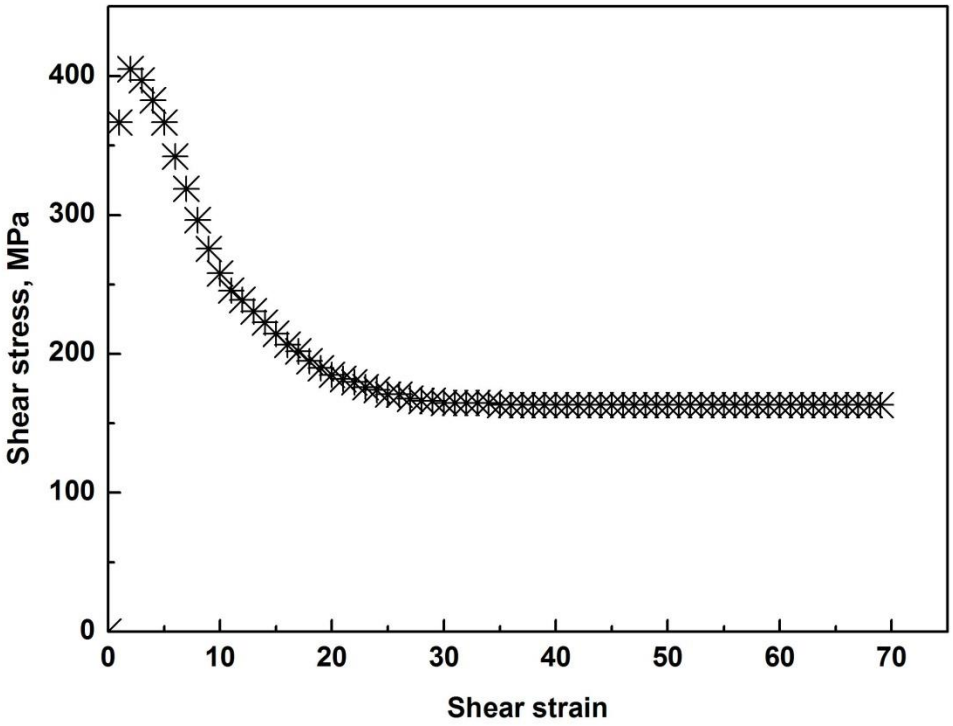

Fig. 2. Experimental shear stress-shear strain curve

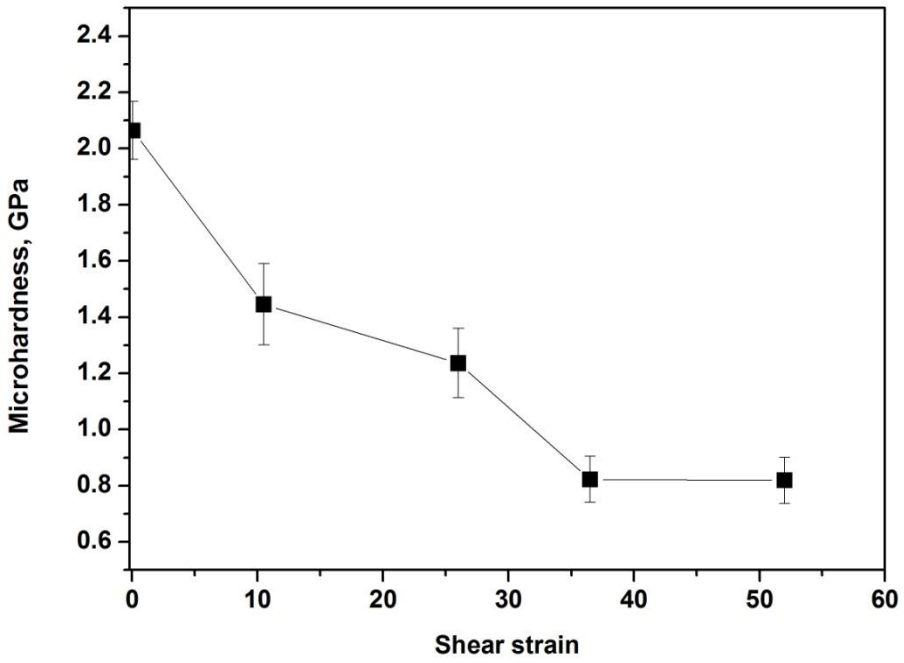

Fig. 3. The hardness measurements at different strain level

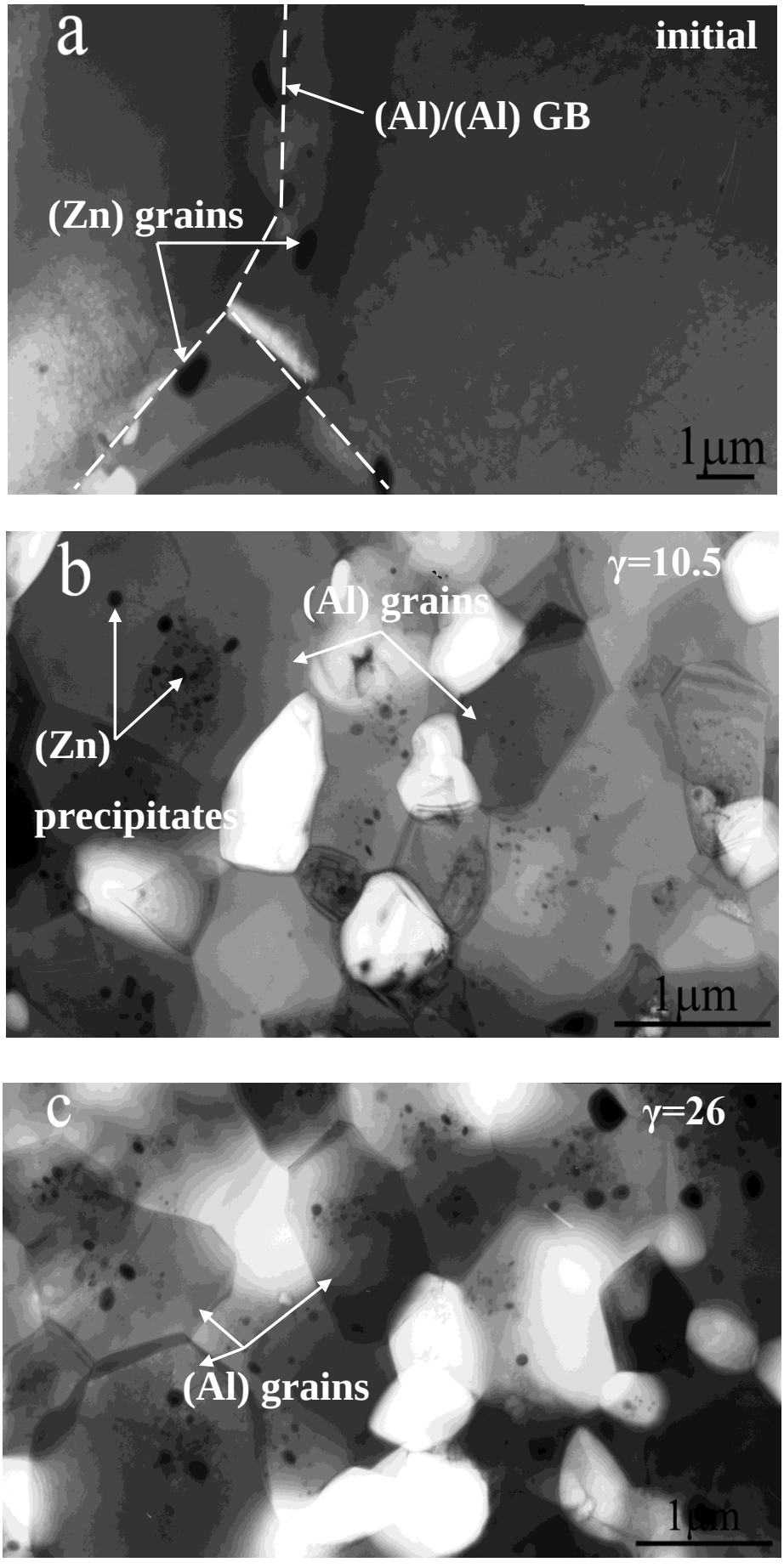
a
initial
(Al)/(Al) GB
(Zn) grains
1μm
b
γ=10.5
(Al) grains
(Zn)
precipitates
1μm
c
γ=26
(Al) grains
1μm

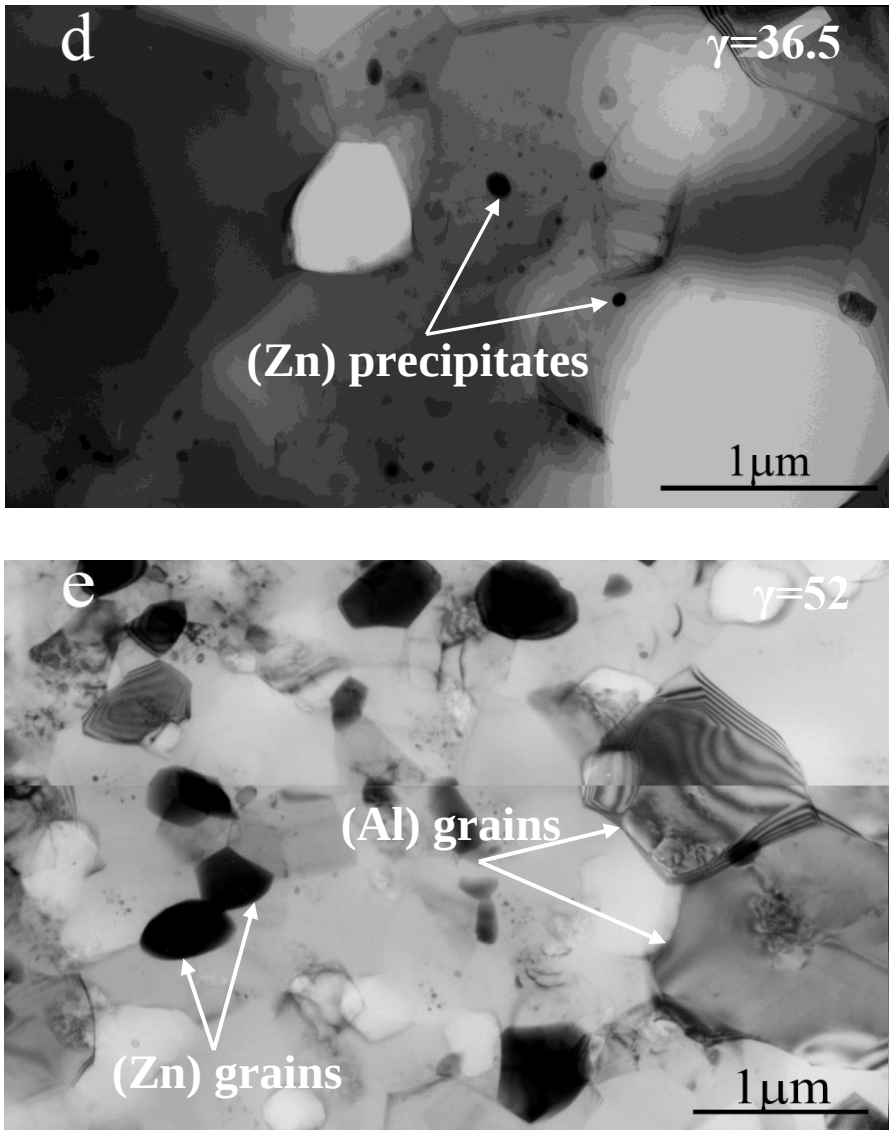

Fig. 4. The microstructural evolution of Al-30wt%Zn during HPT, for the initial state (a) and at different strain level: (b)- $\gamma = 10.5$, (c)- $\gamma = 26$, (d)- $\gamma = 36.5$ and (e)- $\gamma = 52$

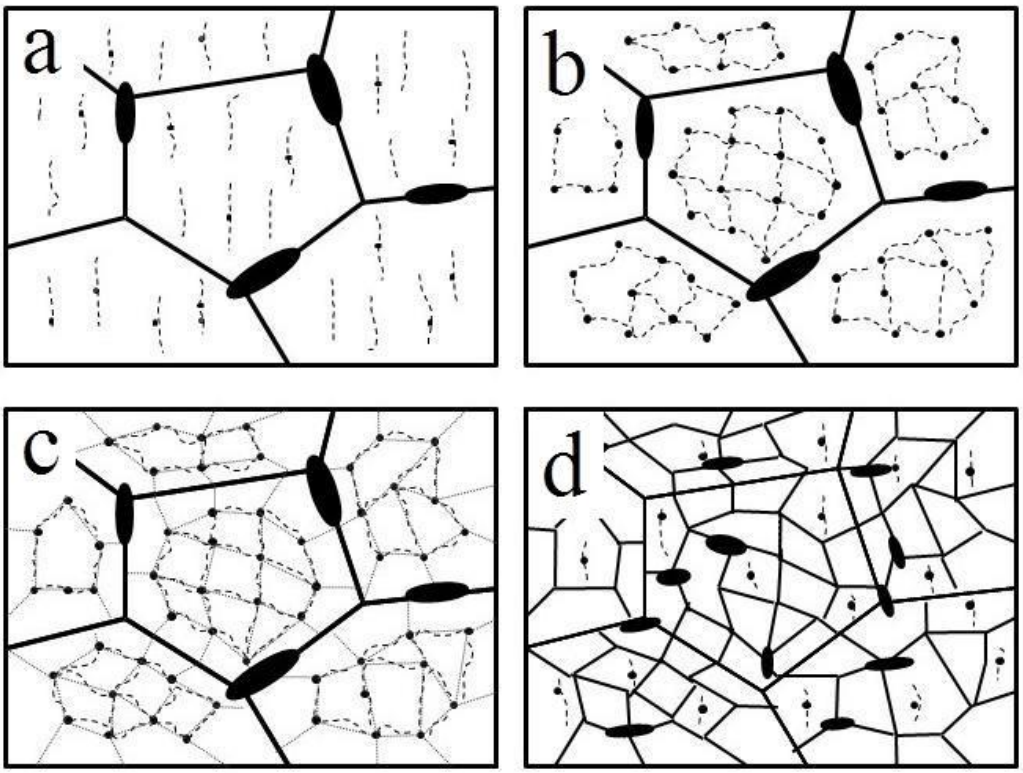

Fig. 5. Schematic view of grain refinement of Al-Zn alloys during HPT process. In this sketch the large black ellipses indicate Zn grains located at the grain boundaries, while the smaller black circles indicate Zn precipitates within the grain. The black dash lines indicate dislocations pinned by precipitates and forming regular arrays in the grains, while the gray lines in Fig. 5c illustrate the division of grains into sub-grains. The continous lines in Fig. 5d demonstrate the new grains after refinement.

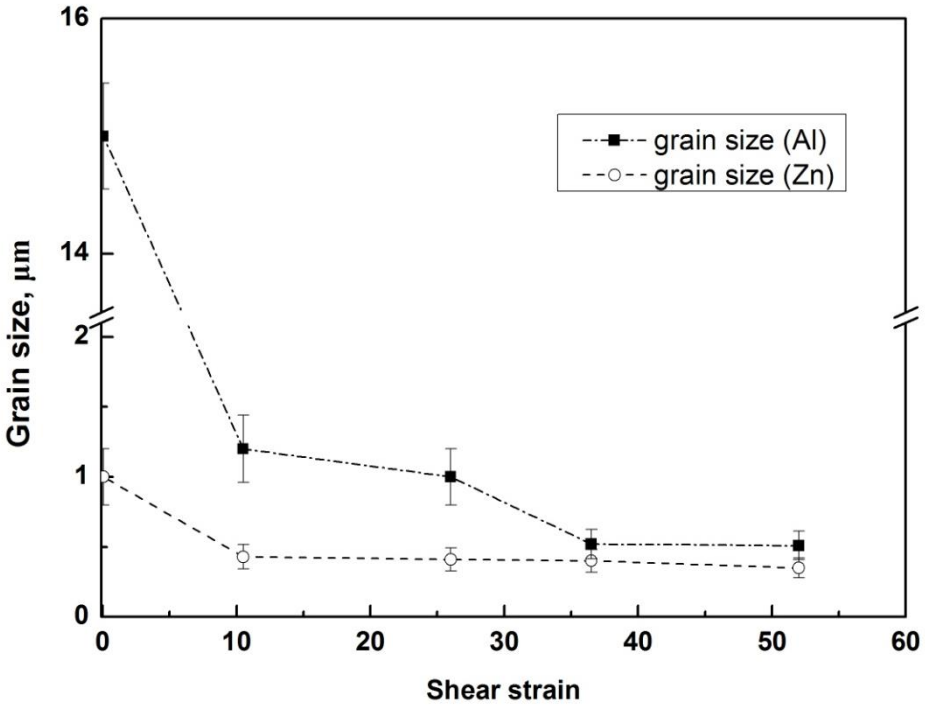

Fig. 6. The evolution of the grain size with the shear strain

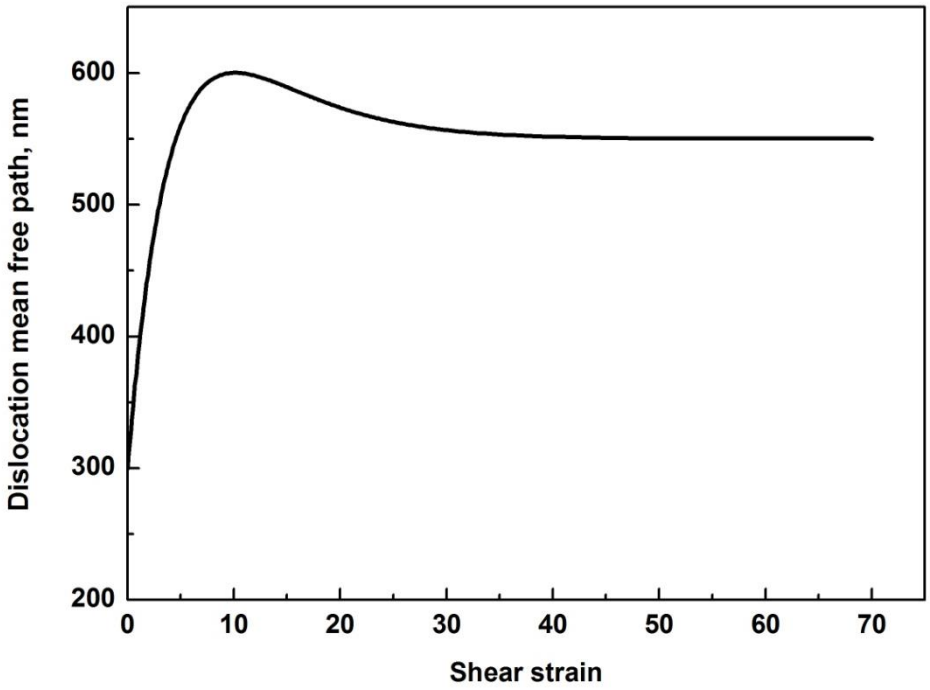

Fig. 7. The calculated evolution of the dislocation mean free path with shear strain

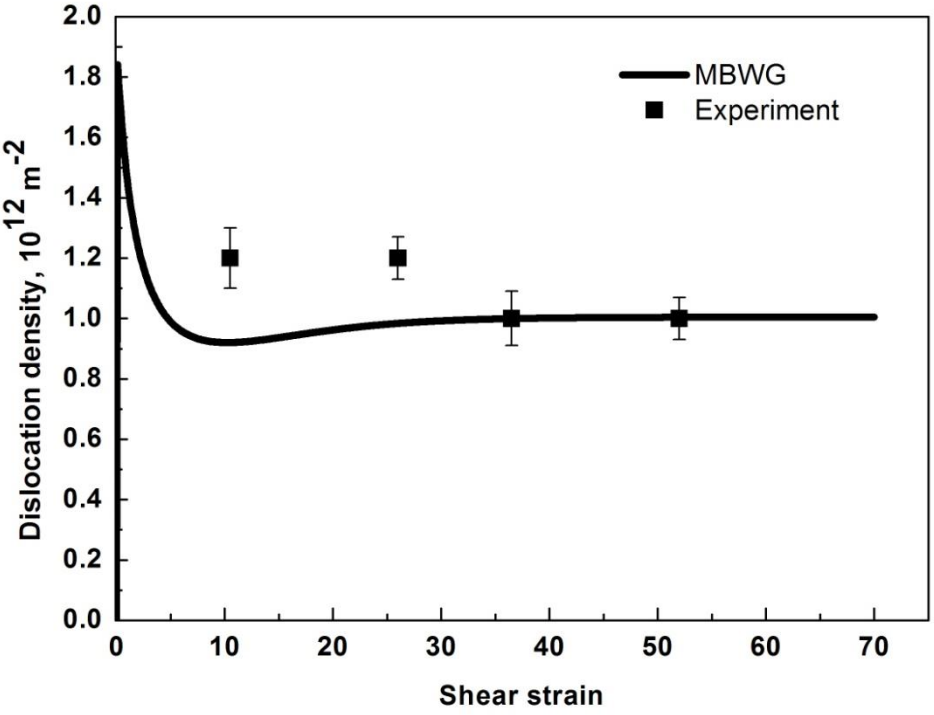

Fig. 8. The experimental and calculated evolutions of the dislocation density with shear strain

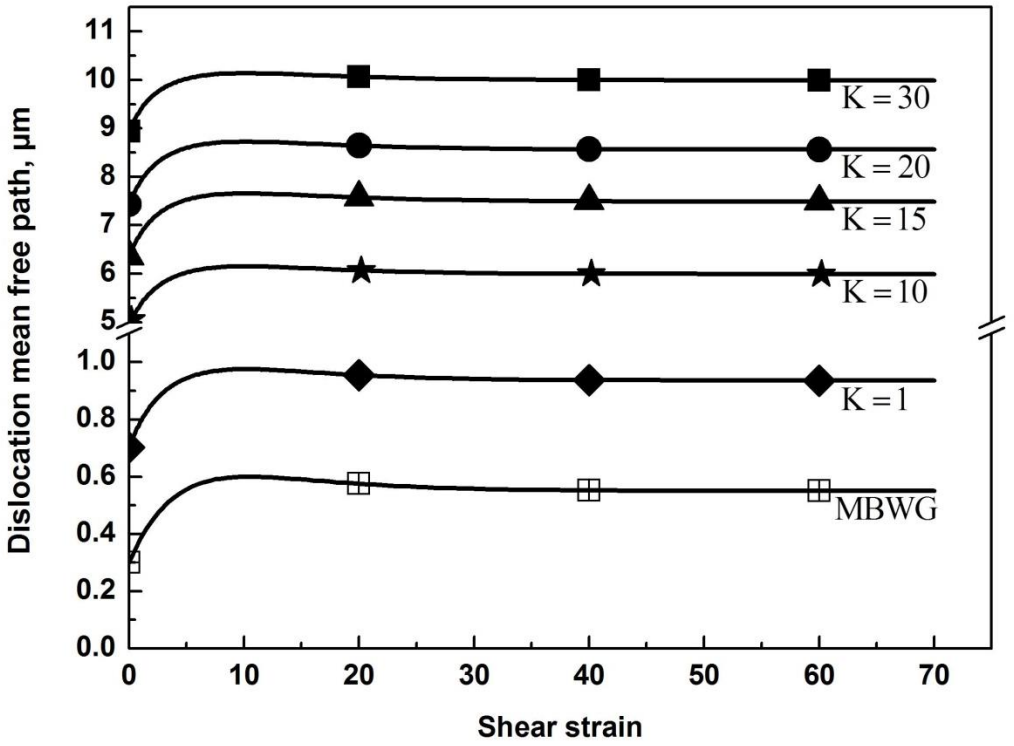

Fig. 9. The comparison of the evolution of dislocation mean free path with shear strain calculated by the approach of Kocks and Mecking (Eq. 17) and MBWG model (Eq. 8)

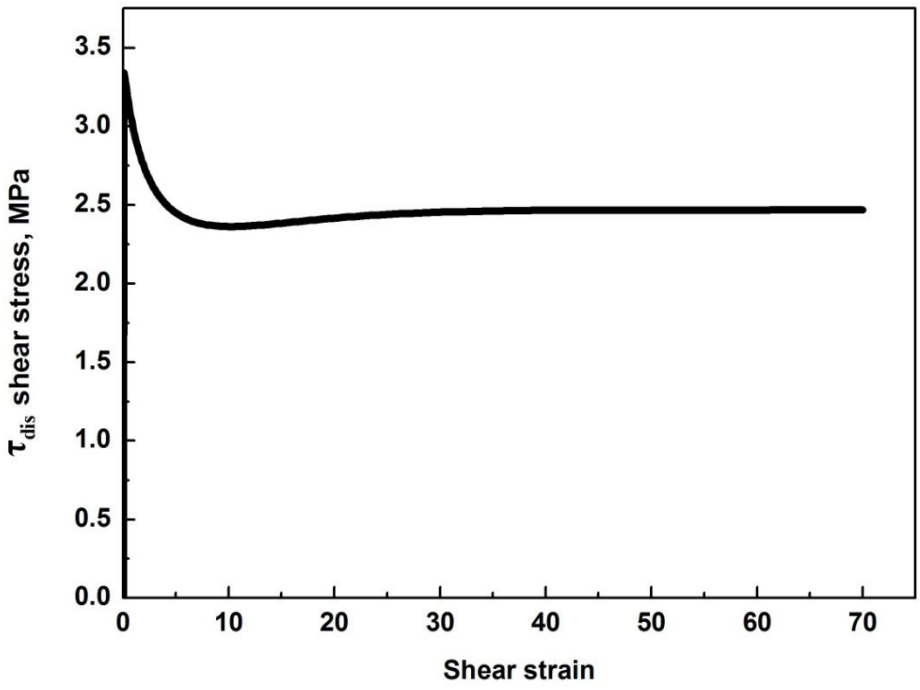

Fig. 10. The calculated evolution of the τ_{dis} shear stress with shear strain

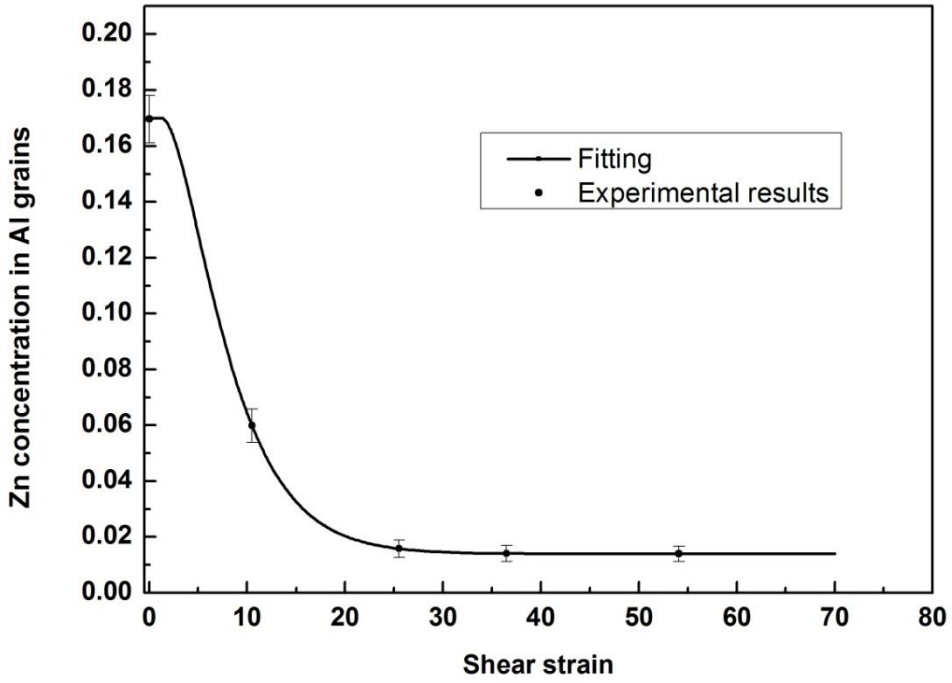

Fig. 11.The evolution of Zn concentration in Al grains with shear strain

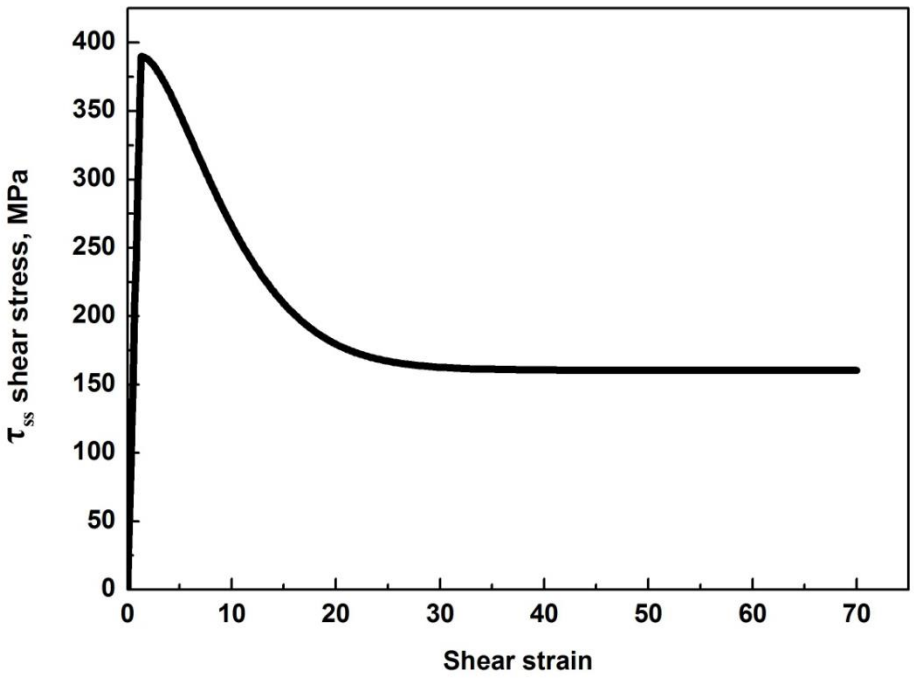

Fig. 12. The calculated evolution of τ_{ss} shear stress with shear strain

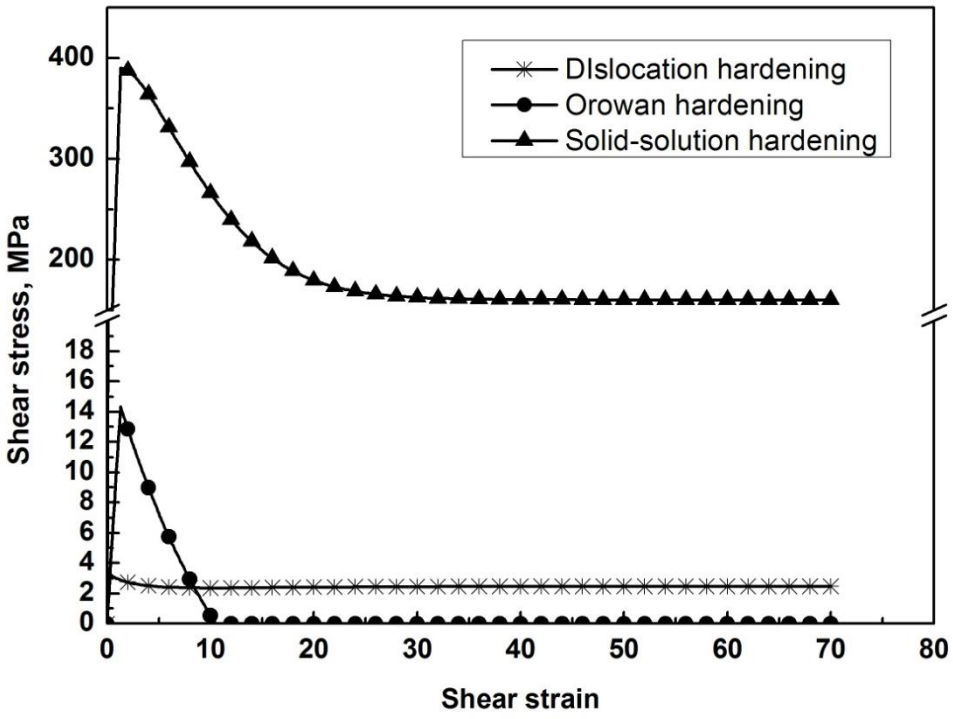

Fig. 13. The comparison of the contribution of different hardening mechanisms

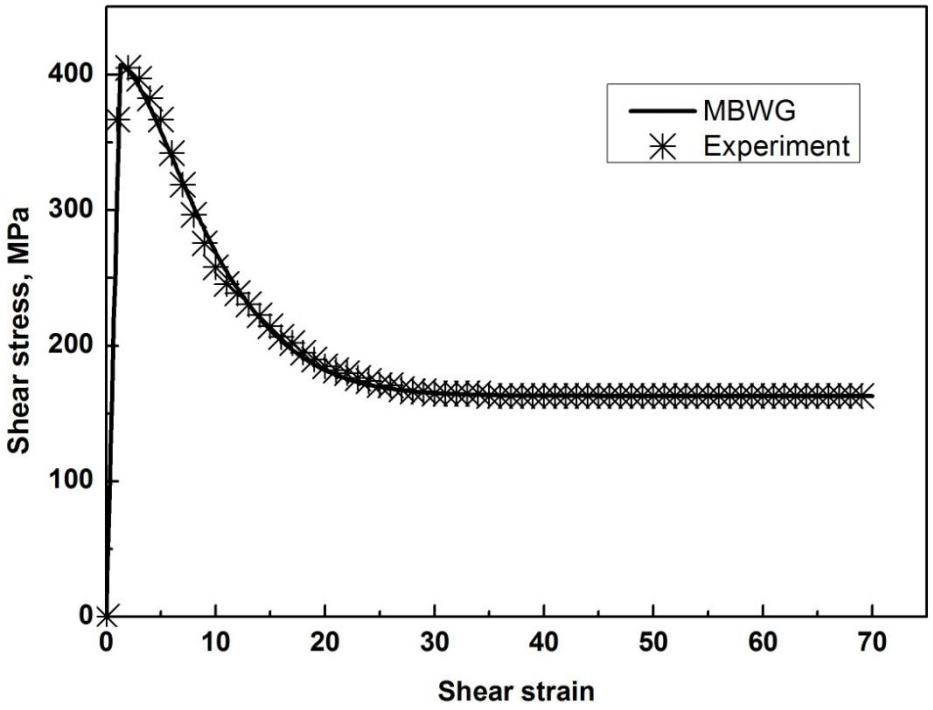

Fig. 14. Comparison between the predicted and experimental shear strain-shear stress curves.

shear strain	lattice parameter, nm
initial	0.40437±0.000023
10.5	0.40471±0.00003
26	0.40485±0.00003
36.5	0.40485±0.00003
52	0.40485±0.00003

Table 1. Lattice parameter of Al-30%wtZn alloy for different shear strains during HPT

	Al-30%wtZn
μ (elastic shear modulus)	26 GPa
b (Burgers vector)	0.287 nm
α (dislocation-dislocation interaction)	0.33
τ_0 (friction stress)	65 MPa
ω_{i} (initial distance between Zn precipitations)	300 nm
L_{max} (maximum distance between Zn precipitations)	600 nm
d_{i} (initial size of Zn precipitations)	20 nm
f (dynamic recovery term)	6330
ρ_0 (initial dislocation density)	0
ρ_{sat} (saturation dislocation density)	10^{12} m^{-2}
c_1 (constant)	1.15
c_2 (constant)	0.242
c_3 (constant)	1.005
c_4 (constant)	0.2964
m (constant)	0.189
n (constant)	0.169
d_e (critical grain size)	1 μm
d_{sat} (saturation grain size)	550 nm
γ_{sat}	26
ΔG (activation energy for dislocations interactions with the solute structures)	2 eV
$\dot{\gamma}_0$ (characteristic strain rate)	10^7 s^{-1}
$\dot{\gamma}$ (shear strain rate)	0.867 s^{-1}
T (temperature)	298 K
k (Boltzmann constant)	1.38×10^{-23} J/K
τ_p (Peierls stress)	3 MPa
Λ (adjustable scaling factor)	2
$\hat{U}$ (characteristic interaction energy between a single solute and a straight dislocation)	0.162 eV
ω_0 (characteristic range for the interaction)	10 Å
v (Poisson ratio)	0.347

Table 2. The parameters of the model